J Mater Sci (2006) 41:6441–6452
DOI 10.1007/s10853-006-0710-7

Analysis of the apparent friction of polymeric surfaces

S. Lafaye · C. Gauthier · R. Schirrer

Received: 22 December 2003 / Accepted: 13 July 2005 / Published online: 19 September 2006

Abstract The apparent friction coefficient is the ratio between the tangential force and the normal load applied to moving body in contact with the surface of a material. This coefficient includes a so-called ''true local friction'' at the interface and a ''geometrical friction'' which is the ploughing effect. The material underneath a moving tip may display various types of behaviour: elastic, elastic–plastic where elastic and plastic strain are present in the contact area, or fully plastic. As is usual in polymers, the material behaviour is time and temperature dependent and may exhibit strain hardening. A surface flow line model of a scratching tip which links the apparent friction to the local friction and contact geometry was recently proposed. An inverse analysis is used in the present work to estimate the local friction from the measured apparent friction and a knowledge of the contact area and tip shape. The polymer true friction coefficient displays temperature and sliding speed dependency, which may be attributed to the surface thermodynamics. It is shown that the local friction depends on the level of strain in the polymer at the contact interface.

Symbols

μ_{app}	Apparent friction coefficient
μ	True friction
f_{ad}	Adhesive friction coefficient
μ_{plough}	Ploughing friction coefficient
f_{visco}	Viscoelastic friction coefficient
f_{plast}	Plastic friction coefficient
F_t	Tangential force
F_{ad}	Adhesive force
F_n	Normal load
τ_{app}	Apparent interfacial shear stress
τ(or τ_{true})	Shear stress at the moving contact area
τ_{plough}	Ploughing shear stress
p_m	Contact pressure
σ_y	Yield stress
p	Local pressure at the contact
p_m/σ_y	Normalised contact pressure
S_n	Real normal contact area
S_t	Tangential contact area
ds	Contact surface element
K	A constant
H	Hardness
tanδ	Loss factor
θ	Half apex angle of the conical tip
ω	Rear contact angle
A,B,C,D	Elementary action integrals of the local pressure and shear
dε/dt (or $\dot{\varepsilon}$)	Mean effective strain rate
V	Sliding speed
l	Scratch contact width
a	Contact radius
R_{tip}	Radius of the tip
T	Temperature
$\vec{x}\vec{y}\vec{z}$	Axes moving with the tip
$\vec{z}$	Axis of the indentation direction
$\vec{\chi}$	Axis of the scratching direction
$\vec{N}$	Elementary normal load vector
$\vec{T}$	Elementary tangential load vector
$\vec{n}$	Normal unit vector
$\vec{t}$	Unit vector tangential to the flow lines

S. Lafaye · C. Gauthier (✉) · R. Schirrer
Institut Charles Sadron, CNRS-UPR 22, 6 rue Boussingault,
F-67083 Strasbourg, France
e-mail: gauthier@ics.u-strasbg.fr

Introduction

After a short review of the relevant scales of friction and of the related analysis, this paper presents an analysis of the apparent friction recorded during scratching of polymers. This apparent friction may be split into two parts: the local friction and the geometrical friction. The major point for the analysis is to take into account the shape of the true contact area between the tip and the surface.

The relevant scales of friction

Figure 1 shows the three relevant scales of friction named macroscopic, local and molecular friction scales. For each scale, a relevant type of friction is associated.

Macroscopic friction scale

The macroscopic scale is that of the relative motion between two macroscopic bodies. The contact area is composed of a large number of elementary discontinuous local contact areas having various geometries. At this macroscopic level, the friction coefficient is one of the physical parameters contributing to the dissipated energy, which is at the origin of the wear phenomena between moving surfaces. Measurements of the macroscopic friction reveal a dependency on temperature and sliding speed and attempts have been made to give a physical sense to this dependency [1, 2]. The first macroscopic contact analysis [3] concerned the static contact of metallic materials, for which adhesion at the interface of the contact could be neglected. These initial studies allowed confirmation of Bowden and Tabor's relations linking the normal load to the real contact area [4] and definition of the conditions for the transition from elastic to elastic–plastic contact. The approach has since been extended to take into account the adhesion [5, 6] and local models have been integrated into the rough static contact model [7].

Local friction scale

At the local scale, the contact area is a smooth planar surface with perfect continuous contact between the bodies. In polymers the local friction presents a peak when the glass temperature transition is reached and the evolution of the friction is comparable to that of the mechanical loss factor tanδ [8]. The origin of this friction peak is attributed to adhesion hysteresis [8, 9] corresponding to the energy dissipation of a loading–unloading cycle. As soon as the friction concerns representative elementary volumes of the material, the notions of contact pressure and contact strain should be taken into account. On this scale [10–12], the test apparatus is a micro-scratch or more recently a nano-scratch apparatus. Briscoe [13] assumed that the energy consumed is mainly located in two zones. The first is the interface, a very thin layer subject to extremely high shear strain, a high strain rate and adhesive slipping. The second zone is spherical and its size is comparable to that of the groove left on the surface. The strain rate of this volume will be lower than that in the interfacial layer. The apparent friction is the ratio between the tangential force and the

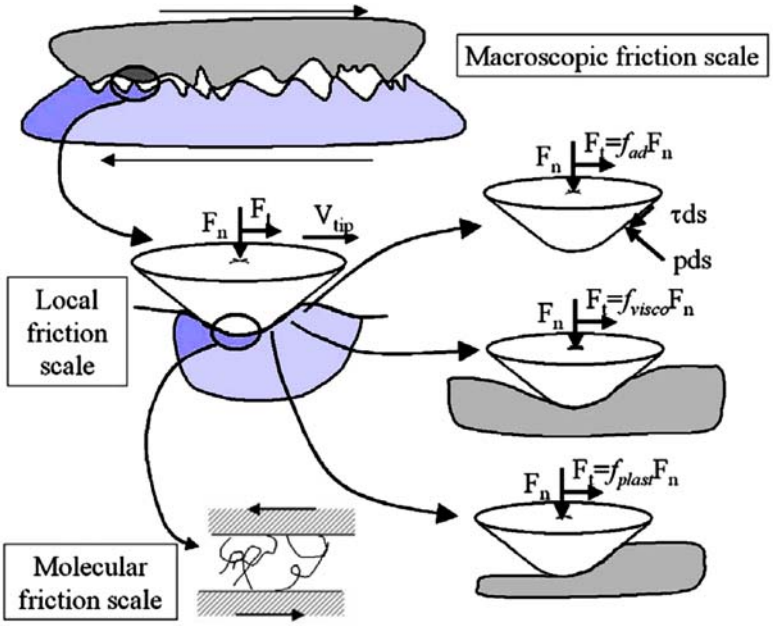

Fig. 1 The three relevant scales of friction named macroscopic, local and molecular friction scales

normal load and there is competition in this friction between an adhesive term and a ploughing term [14]. The latter may be decomposed into one term due to the viscoelasticity and another due to the plasticity. Hence the friction may be written as

$$\mu_{app} = f_{ad} + f_{visco} + f_{plast} \quad (1)$$

Molecular friction scale

At the molecular level and using a spherical tip having a large radius (typically a surface force apparatus or a pin on disc apparatus), sliding studies on polydiméthylsiloxane (PDMS) [15] show that the friction depends on the sliding speed in relation to the interpenetration of the macromolecular chains, while the adhesion hysteresis is linked to the dissipated work when the chains remain in their original state. This penetration decreases with the sliding speed to disappear when the network begins to slide on a solid-like brush. The brush is solid-like if the friction decreases to tend to an asymptotic value, or liquid-like if the friction increases with the sliding speed [8, 16]. Friction tests performed under an AFM allowed study of the friction at the level of the polymer chains. On this scale, the AFM is used to extract a molecular chain. The AFM is also employed to measure the friction force, to study nano and micro scratches and to determine the surface topography of a sample [17, 18]. However, the results obtained on this scale are sometimes unpredictable. The friction may be independent of the sliding speed [19], while the depth of the groove can vary with the scratching speed [20]. It has been observed that the friction is stable only after a sliding length approximately equal to the contact width [18].

The relevant types of friction

Adhesive friction

The components of the friction are generally analysed by tests, which allow separate assessment of each elementary friction coefficient. The Bowden and Tabor [21] mono-contact analysis permits linkage of the adhesive friction to the adhesive shear for a plastic contact. If the angle between the front face of the moving tip and the surface is small, then the adhesive force is

$$F_{ad} = \tau S_n \quad (2)$$

and the normal load is

$$F_n = pS_n \quad (3)$$

where, τ is the shear stress at the moving contact area; p is the local pressure at the contact which is equal to the hardness of the softer material; S_n is the real contact area.

In these conditions the adhesive term f_{ad} of the friction becomes

$$f_{ad} = F_{ad}/F_n = \tau/p \quad (4)$$

At temperatures below the glass temperature and using tests analysing the sliding of a ball on polymer films deposed on hard substrates, Briscoe and co-workers [13, 22, 23] has shown that the interfacial shear may be written as

$$\tau = \tau_0 + \alpha p \quad (5)$$

The adhesive term of the friction is written as

$$f_{ad} = \frac{\tau_0}{p} + \alpha \quad (6)$$

where τ_0 is usually equal to one MPa and α lies in the range 0.08–0.6 for a large variety of solid polymers [13]. This model is derived from experimental tests and seems to indicate that the friction decreases as the contact pressure increases. Briscoe et al. has also examined the friction during sliding contact between a hot steel ball and a poly(ether-ether ketone) surface [24]. The evolution of the friction as a function of temperature is explained as resulting from competition between the evolution of the shear stress and the elasticity modulus as a function of temperature. Reduction of the friction evolution to a simple adhesion process is not consistent because the viscoelasticity acts on the contact shape and the adhesive friction.

Ploughing friction

The viscoelastic origin of the ploughing component of the friction is given by Moore [14]. The influence of strain hardening has been demonstrated experimentally and using numerical simulation [11, 25]. But there is at present no relationship linking the friction to the contact shape as the behaviour of the contact evolves from elastic to plastic.

Viscoelastic friction

Bulgin et al. [26] and Moore [14] consider that during continuous sliding contact on a polymeric surface, there is alternately adhesion between the polymer and

the moving tip for a short time and then relaxation after a certain displacement distance. A Voigt model provides a relation between the friction coefficient and the loss factor

$$f_{\text{visco}} = \frac{K}{H}\tan\delta \tag{7}$$

where K is a constant and H the hardness. In rolling tests on an elastomeric material, Moore reported a friction peak in phase with the loss factor peak tanδ. Bueche and Flom [27] had already noted in 1958, in tests of the sliding of a steel ball on solid polymeric surfaces (poly(methylmethacrylate) and polyethylene), this similitude between the friction and loss factor peaks. Many authors have observed similar behaviours in tests of a steel ball rolling on polytetrafluoroethylene (PTFE) or a steel ball sliding on rubber [27–29]. In these sliding tests on the millimetre scale, the surface is generally lubricated to minimise the adhesive friction, which lends more importance to the ploughing part of the friction.

Plastic friction

The f_{plast} term due to plasticity is usually evaluated for a perfectly dissymmetric contact from the plastic model given by Bowden and Tabor [21]. Fig. 2 shows that this model applies to a perfectly conical tip and considers the ratio between the frontal projected and horizontal contact areas. If the half apex of the conical tip is θ, the plastic friction is

$$f_{\text{plast}} = 2/\pi\cot\theta \tag{8}$$

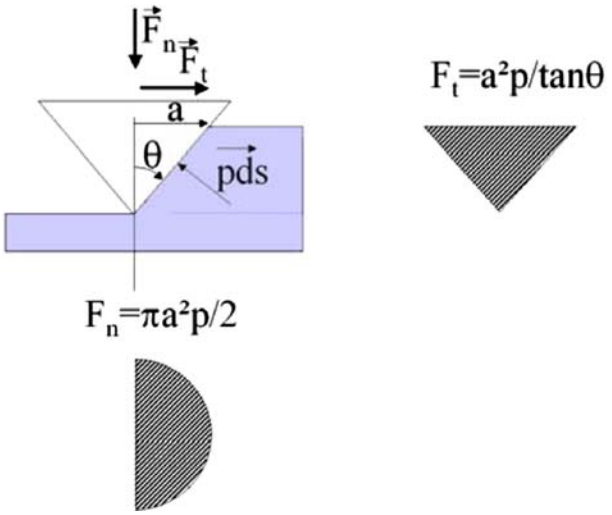

Fig. 2 Plastic friction model applied to a perfectly conical tip and a rigid perfectly plastic behaviour

This relationship suggests that the plastic term of the friction coefficient depends only on the tip geometry and does not take into account the elastic–plastic behaviour of the material or the contact shape, which depends on partial elastic unloading. Tabor's model cannot be applied to viscoelastic–plastic materials having a low ratio of the elastic modulus to the yield stress, as is the case for polymers. Thus, the scratching of polymers shows elastic unloading which partially recovers the rear contact [30]. Furthermore, for a viscoelastic–plastic contact where elastic and plastic strains exist in the material surrounding the contact tip, this elastic unloading can be very important. In the case of a viscoelastic contact, the contact area becomes quasi symmetric. Fig. 3 shows four in-situ photographs of the contact area obtained with an experimental apparatus developed in our laboratory [12]. Four shapes of the contact between a spherical tip and a poly(methylmethacrylate) surface are visible on these pictures. Fig. 3a corresponds to a quasi-elastic contact with a relaxation time equal to the contact time, where incipient interference fringes reveal a slight dissymmetry. Fig. 3b depicts a viscoelastic contact where the groove relaxes after a time interval longer than the contact time. In the elastic–plastic contact of Fig. 3c, the strain under the contact is not completely plastic, there is no frontal push pad and the lateral pad of the groove appears only after elastic unloading of the contact strain. Finally, Fig. 3d shows a plastic contact where the frontal push pad and lateral pads form a continuous cord.

Recent developments in models of the ploughing friction

Generalisation of Tabor's solution

Bucaille et al. [31] have generalised Tabor's approach to take into account the rear contact defined by the angle ω (Fig. 4a)

$$\mu_{\text{plough}} = \frac{2}{\pi}\cot\theta\left(\frac{\pi\sin(\omega+\pi/2)}{\pi+2\omega}\right) \tag{9}$$

However, a simple rear contact angle does not separate the different mechanical components (viscoelasticity, or elastic unloading after an elastic–plastic or fully plastic contact), which contribute to the rear contact and decrease the friction. This model of the ploughing friction allows one to obtain the limiting cases for $\omega = 0$ and $\pi/2$, but it neglects the triangular sector inside the dorsal angle (Fig. 4a).

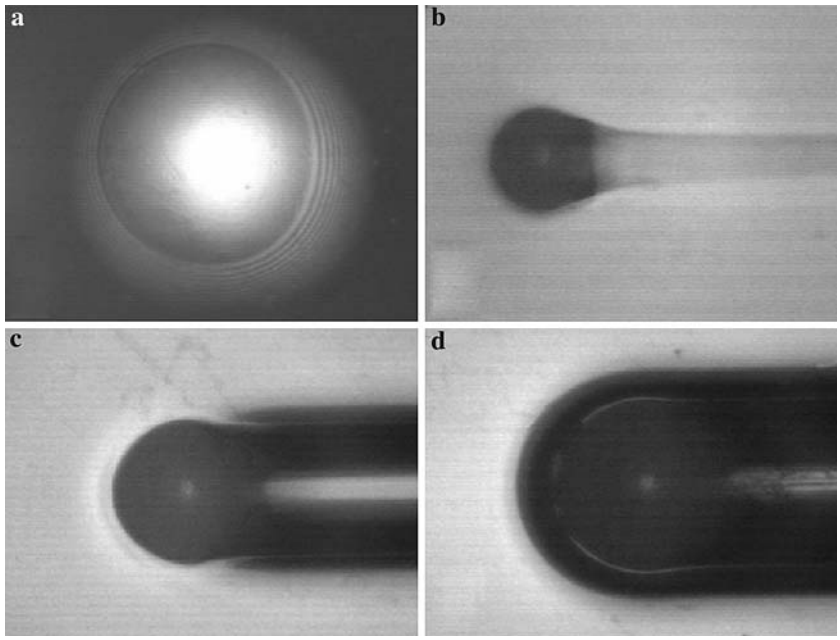

Fig. 3 Typical photographs of the true contact area during scratching of a PMMA surface with a spherical tip. The tip scratches the surface from right to left

Observation of the plastic groove produced by moving conical tips having an apex angle of more than 90° (Fig. 2b) has shown that this triangular contact area should be taken into account. The ploughing friction coefficient is estimated as the ratio between the cross section of the groove (in grey on Fig. 5) and the normal section of the contact area. This cross section is given by the intersection between the cone of the tip and a plane parallel to the axis of the cone, which is a hyperbola. The equation of the ploughing friction depends on the apex angle θ and the rear angle ω, and details of the calculation are given in an appendix. An approximate calculation allows estimation of the cross section as a triangular section having a width at the base equal to the rear width of the contact and a height equal to that of the hyperbola previously defined, as indicated in Fig. 5. The ploughing part of the friction including the rear angle and this approximation is

$$\mu_{\text{plough}} = \frac{2}{\pi}\cot\theta\left(\frac{\pi\cos\omega(1-\sin\omega)}{\pi+2\omega+\sin 2\omega}\right) \tag{10}$$

For $\omega = 0$ Eq. 10 is equal to Tabor's friction coefficient, and for $\omega = \pi/2$ the ploughing friction is null. Fig. 6 presents the evolution of the ploughing friction in the three generalised models based on Tabor's relation (triangular, hyperbola and Bucaille models) as a function of the rear angle ω. This figure shows that a small discrepancy in estimation of the true contact area for a conical tip geometry can lead to important shifts in the ploughing friction coefficient. The analysis of

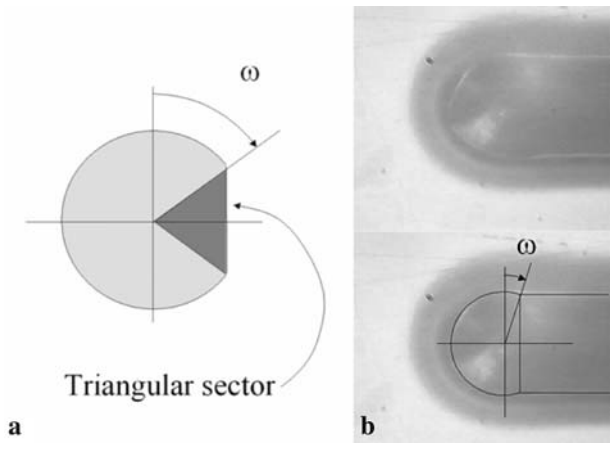

Fig. 4 (**a**) Model of the contact area showing the triangular sector; (**b**) Photograph of the true contact area during scratching of a PMMA surface with a 120° apex angle tip and estimation of the shape of the contact area. The triangular sector has to be taken into account to determine the contact area

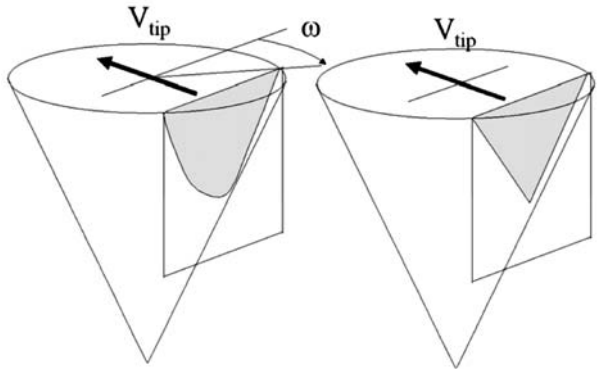

Fig. 5 Geometrical definition of the rear contact and the cross section used to estimate the ploughing friction. Exact solution on the left and triangular solution on the right

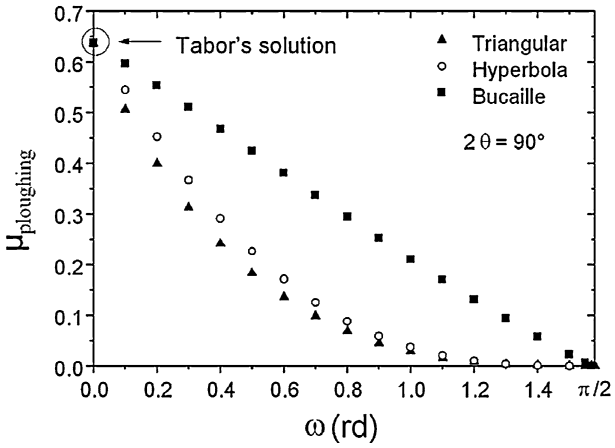

Fig. 6 Evolution of the generalised ploughing friction coefficient as a function of the rear angle for a 90° cone angle. Comparison of the exact solution, the triangular approximation and the Bucaille solution. At a rear angle of zero, all three solutions give Tabor's relation

experimental results described in section four of the present work used a flow line model [32] based on the hyperbolic cross section of the groove.

Inverse determination of the true local friction from experimental results and using a flow line model

Experimental photographs show that the true contact area is the sum of a front area (half disc of radius a_f) and a rear area (part of the rear half disc). The difficulty is to account this rear contact in order to relate the true and ploughing frictions to the measured apparent friction. In a previous work [32], three types of flow lines were tested in a new analytical simulation model designed to determine the apparent friction coefficient of conical and spherical tips scratching a surface. The input data required by the simulation are the true contact area, the true local friction coefficient and a model of the pressure acting on the contact surface. The type of pressure distribution introduced into the model does not significantly modify the results of the simulation.

The elementary local normal and tangential forces due to material flow acting on a contact surface element ds of the tip are

$$\vec{N} = -p\mathrm{d}s\vec{n} \tag{11}$$

$$\vec{T} = \tau\mathrm{d}s\vec{t} \tag{12}$$

where $\vec{n}$ and $\vec{t}$ are units normal and tangential to the flow lines vectors and p and τ the local normal pressure and shear stress. The mean macroscopic values of the forces may be defined by

$$\vec{F}_\mathrm{n} = F_\mathrm{n}\vec{z} = [(Ap + B\tau)S_\mathrm{n}]\vec{z} \tag{13}$$

$$\vec{F}_\mathrm{t} = F_\mathrm{t}\vec{x} = [(Cp + D\tau)S_\mathrm{n}]\vec{x} \tag{14}$$

with

$$A = \frac{1}{S_\mathrm{n}}\int \vec{n}\cdot\vec{z}\mathrm{d}s \quad B = -\frac{1}{S_\mathrm{n}}\int \vec{t}\cdot\vec{z}\mathrm{d}s$$
$$C = \frac{1}{S_\mathrm{n}}\int \vec{n}\cdot\vec{x}\mathrm{d}s \quad D = \frac{1}{S_\mathrm{n}}\int \vec{t}\cdot\vec{x}\mathrm{d}s \tag{15}$$

where $\vec{x}$ and $\vec{z}$ are unit scratching and indentation axes and S_n is the normal projected contact area. The true local friction μ is defined as $\mu = \tau/p$ and therefore

$$\frac{F_\mathrm{t}}{F_\mathrm{n}} = \mu_\mathrm{app} = \frac{C + D\mu}{A + B\mu} \tag{16}$$

Then, resolving this equation relating the true and apparent frictions requires calculation of the four integrals A, B, C and D, which are the elementary action integrals of the local pressure and shear, together with a knowledge of the rear angle ω, the real contact area and the geometry of the tip. A, B, C and D take into account the macroscopic contact shape [32]. In the case of frictionless scratching of plastic materials, the apparent friction is equal to the ratio between C and A, and the result fits well with the well known analytical solutions for a conical tip [21] or a spherical tip [33].

Conversely, if the apparent friction coefficient and shape of the tip are known from experimental data, the true local friction may be calculated from the Eq. 16 thus

$$\mu = \frac{A\mu_\mathrm{app} - C}{D - B\mu_\mathrm{app}} \tag{17}$$

Experimental apparatus and test conditions

The scratch apparatus, described in detail by Gauthier and Schirrer [12], is based on a commercial servo-mechanism bearing a small transparent environmental chamber, which contains the sample and the moving tip. A built-in microscope allows in-situ control and analysis of the groove left on the surface, which is possible due to the transparency of the tested polymers. Scratch tests may be performed over a wide range of speeds (1 μm/s to 15 mm/s) and within a temperature range covering the α and β transitions of common polymers (– 70 °C to +120 °C). Control of the moving tip and recording of the load, speed and

temperature are computer driven. The normal load applied to the tip can be selected from 0.05 N to 5 N. The tip starts at the lowest velocity and accelerates stepwise up to the highest velocity. At each speed step, it moves over a distance of at least 1 mm in order to obtain a groove which can be easily measured and photographed in-situ. The test parameters are the normal load, tip geometry, temperature and sliding speed, while the measured parameters are the tangential force, groove geometry and true contact area. According to the adjustment of the normal load, temperature, strain rate and tip geometry, the contact between the hard tip and the polymer surface may be elastic, or may generate a viscoelastic groove or a plastic scratch. In the case of viscoelastic sliding, the groove left on the surface relaxes within a time comparable to the contact time. When a viscoelastic–plastic contact exists, the material in the contact area blends elastic and plastic strains and there is bulk elastic unloading and partial recovery of the depth of the groove after passage of the tip. During viscoplastic scratching, the material under the contact surface is mainly subject to plastic strain.

Two materials were used in this study, a commercial grade of cast poly(methylmethacrylate) (PMMA) and an amorphous thermoset resin called CR39 (diethylene glycol bis(allyl carbonate)). The Young's moduli E of CR39 and PMMA are typically 2 and 3.3 GPa, respectively, at 20 °C and 1 Hz. The glass temperature of CR39 lies at about 70 °C and that of PMMA at about 120 °C. Scratch test samples were plates a few millimetres thick.

A typical procedure was used to carry out the friction tests. After cleaning the tip and the sample with alcohol and drying, a preliminary test was performed to age the surface of the tip with the polymer, which is necessary to obtain reproducible measurements. In the present experiments, the grooving tips were of variable geometry. In tests on CR39, we used a conical tip with an apex angle of 90° and a tip radius of 110 μm. A constant normal load of 1 N was applied to the tip sliding over the CR39 surface and the temperature was in the range – 50 °C to +100 °C and the sliding speed was in the range 1 μm/s to 15 mm/s.

The tip used for scratch tests on PMMA was conical with an apex angle of 120° and a tip radius of 30 μm. In tests performed at 110 °C, the normal load was increased linearly and the sliding speed logarithmically: at 1 μm/s the normal load was 0.1 N while at 0.1 mm/s the load tended to 1.5 N. At higher sliding speeds, the material was below its glass temperature and behaved like a solid polymer. In tests performed at temperatures in the range – 50 °C to +110 °C, the normal load was adjusted to give a constant initial contact width typically equal to 100–150 μm during the first speed step and then kept constant. Other sliding tests on PMMA were carried out at room temperature, using a constant normal load adjusted in the range 0.2–2 N and ball tips of various radii (1500, 790 and 240 μm) in order to scan a wide range of contact strains.

Analysis of experimental results

Apparent friction and true local friction

Figure 7 shows the apparent friction as a function of sliding speed for three different temperatures and Fig. 8 the apparent friction as a function of temperature for a sliding speed of 12 μm/s. The apparent friction presents a large peak at about 60 °C and may be termed the solid or liquid friction, depending on the decreasing or increasing trend as a function of sliding speed.

Figure 9 presents the rear angle ω as a function of temperature for a sliding speed of 12 μm/s and Fig. 10 the contact width as a function of temperature for the same sliding speed. The rear angle decreases as the temperature reaches the glass temperature and then increases after the transition.

The flow line model [32] allows one to estimate the true local friction from the apparent friction and the shape and size of the contact. Fig. 11 shows the apparent and true local frictions as a function of temperature. The apparent friction presents a large peak at 50–60 °C, which is due to modification of the contact geometry (rear angle ω and contact width) and related

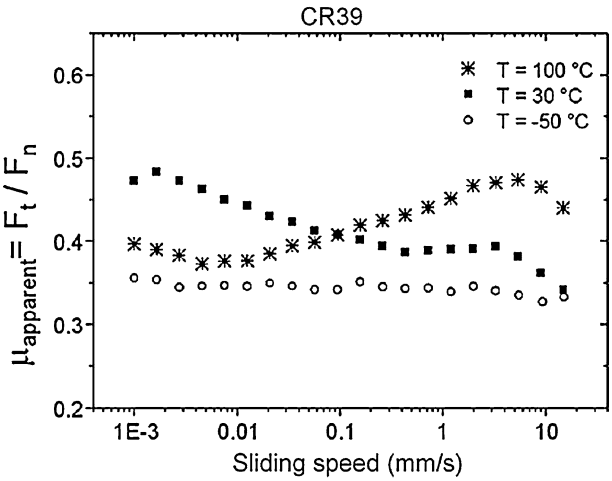

Fig. 7 Apparent friction as a function of sliding speed for three temperatures in a scratch test on CR39 (Rtip = 110 μm)

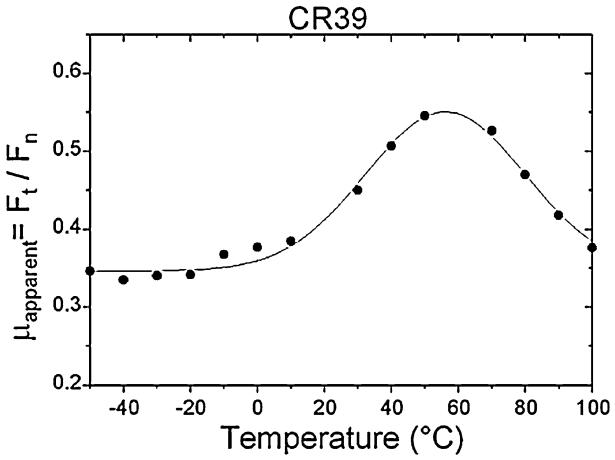

Fig. 8 Apparent friction as a function of temperature for a sliding speed of 12 μm/s in a scratch test on CR39

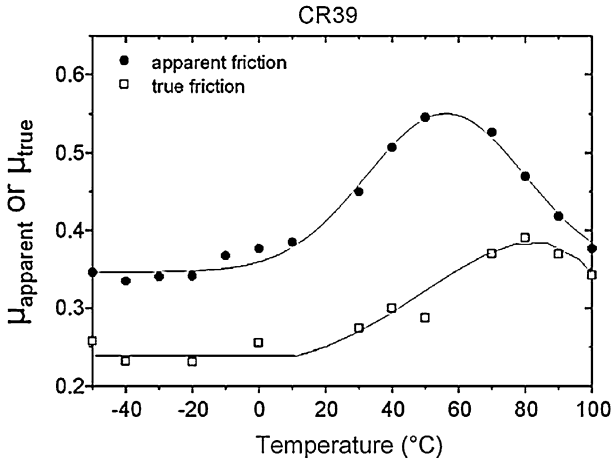

Fig. 11 Apparent and true local frictions as a function of temperature for a sliding speed of 12 μm/s in a scratch test on CR39

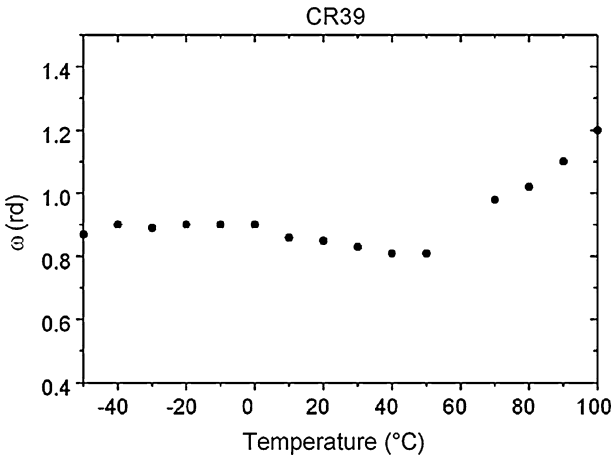

Fig. 9 Rear angle as a function of temperature for a sliding speed of 12 μm/s in a scratch test on CR39

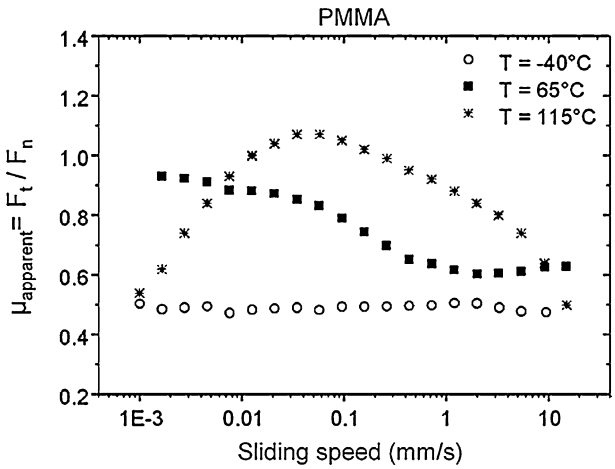

Fig. 12 Apparent friction as a function of sliding speed for three temperatures in a scratch test on PMMA (conical tip)

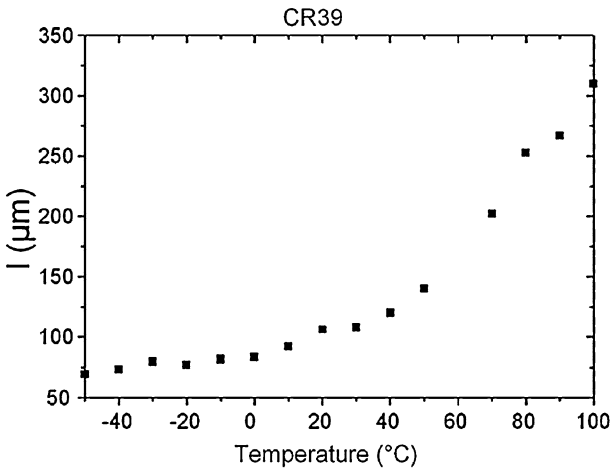

Fig. 10 Contact width as a function of temperature for a sliding speed of 12 μm/s in a scratch test on CR39

to the bulk behaviour of the polymer during the scratch test, while the true friction displays a small peak at the glass temperature due to a tack phenomenon, related to the interfacial behaviour.

A similar analysis of scratch tests on PMMA gives the same results for the true local friction at a sliding speed of 16 μm/s. Fig. 12 depicts the apparent friction as a function of sliding speed and Fig. 13 the estimated true local friction as a function of temperature.

On these two materials, the observed contact shapes display dissymmetry arising from plastic strain above the glass transition.

Loss factor and apparent and true local frictions

In Fig. 14 the loss factors of CR39 and PMMA obtained by mechanical spectrometry are plotted as a

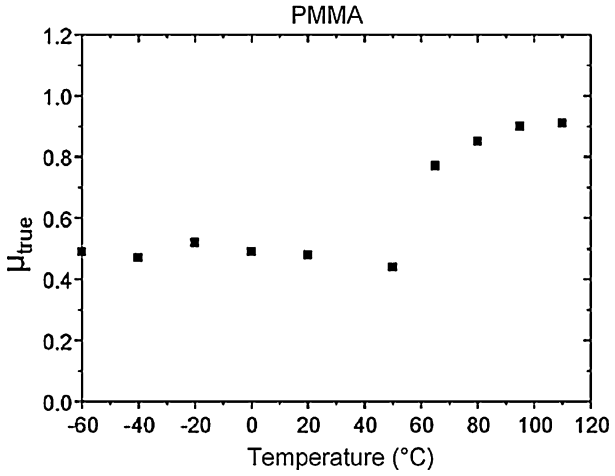

Fig. 13 True local friction as a function of temperature for a sliding speed of 16 μm/s in a scratch test on PMMA

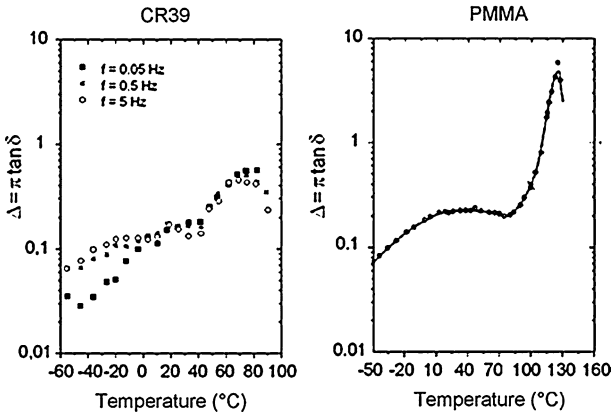

Fig. 14 Logarithmic decrements or loss factors of CR39 (left) and PMMA (right) as a function of temperature [34], as determined by mechanical spectrometry at three test frequencies

function of temperature for three frequencies. CR39 presents a large peak at about 70 °C, which corresponds to the α transition associated with the glass transition of the polymer. Although the beta peak of the loss factor is similar for both materials, the alpha peak is higher in PMMA than in CR39.

These results confirm the correlations reported in the literature between the sliding or rolling friction and the loss factor. Our data further indicate that the rolling friction is comparable to the ploughing friction and originates from the shape of the contact. The ploughing friction originates from the bulk response of the polymer. A non-lubricated sliding friction may be compared to the true local friction and responds to the behaviour of the interfacial layer as suggested by Briscoe.

Normalised local friction on PMMA and CR39

The amplitude of the local friction peak is more important for PMMA than for CR39. Fig. 15 shows the evolution of the true local friction peaks of CR39 and PMMA as a function of the distance from the glass transition temperature. In both cases, the local friction was normalised by the asymptotic value obtained at low temperature. The normalised friction is 50% higher on PMMA than on CR39 once the glass transition is reached. Above the glass transition, tests on PMMA are very difficult to perform because this polymer is not a thermoset resin and its Young's modulus is very low at temperatures exceeding the glass temperature.

As seen in Fig. 14, the loss factor of PMMA is about one order of magnitude greater than that of CR39 once the glass transition is reached. This similarity between the α peak amplitudes of the loss factor and the normalised friction confirms the influence of a molecular mechanism at the origin of the true local friction.

Scission master curves

The mechanical properties of polymeric materials are usually stress and temperature activated. In the case of polymer scratching, Briscoe et al. [35] has introduced the mean effective strain rate $d\varepsilon/dt$, which is the ratio of the sliding speed (V) to the scratch contact width (l) observed post-mortem

$$d\varepsilon/dt = V/l \tag{18}$$

This definition has been used to plot scratch hardness master curves for PMMA [12]. Briscoe and Tabor [22] have further defined the apparent interfacial shear

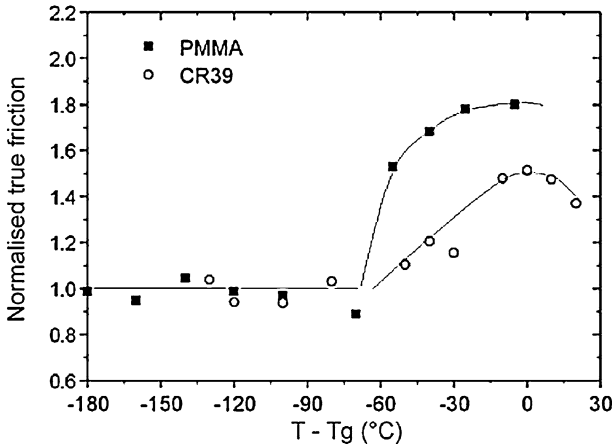

Fig. 15 Normalised true local friction on CR39 and PMMA as a function of the glass transition shift

stress on polymeric films as the ratio of the tangential force to the normal contact area $\tau_{app} = F_t / S_n$. Fig. 16 presents master curves for the apparent shear stress and contact pressure for PMMA as a function of strain rate and temperature in scratch tests with the conical tip. The master curves are plotted at a reference temperature of 20 °C and show an activation energy of about 85 kJ/mol and an activation volume of about 0.4 nm^3. At low temperatures (equivalent to high strain rate), the apparent shear stress and contact pressure vary linearly with the logarithm of $d\varepsilon/dt$ and hence the apparent shear stress depends linearly on the contact pressure.

The apparent shear stress may be split into a ploughing component and a true shear component. The latter is the product of the true friction and the contact pressure

$$\tau_{true} = \mu_{true} \times p \tag{19}$$

and the ploughing shear stress may then be defined as

$$\tau_{plough} = \tau_{app} - \tau_{true} \tag{20}$$

As seen in Fig. 17, the master curves for the ploughing and true shear stresses on PMMA plotted as a function of strain rate at 20 °C display three domains. At low strain rate (or high temperature), the contact is relatively symmetric and both the ploughing stress and the shear stress are low. At high strain rate (or low temperature), the contact is asymmetric and both the ploughing stress and the shear stress increase with the logarithm of $d\varepsilon/dt$. At intermediate strain rate or temperature the effect of the tack leads to a local peak in the shear stress. The effect of the high true friction due to tack observed Fig. 15 on the shear line analysis is less marked in the case of the true shear analysis. This phenomenon occurs when the contact pressure becomes small (less than 50 MPa) and thus has little effect on the true shear stress, which is then less than 50 MPa. The ploughing shear stress master curve presents a peak at about 60 °C (strain rate about 1E-4 s^{-1}). If the shear stress master curve reveals the existence of a thermally activated phenomenon, one may see that a direct representation of the true local friction is more interesting as it highlights the presence of peaks at the glass transition temperature.

Relation between true local friction and strain

Yields stress tests were performed in compression at several temperatures and strain rates. The experimental set-up was based on the moving cross head of an Instron 4502 tensile machine and the whole apparatus was enclosed in an Instron environmental chamber. The strain was limited to 20% in these tests. Cylindrical samples 12.5 mm long and 5 mm in diameter were employed and tests carried out between – 20 °C and 90 °C at four strain rates between 10^{-4} s^{-1} and 10^{-1} s^{-1} allowed estimation of the yield stress over a wide range of scratching speeds and temperatures. The normalised contact pressure (p_m/σ_y) is the ratio of the contact pressure to the yield stress determined at the same strain rate and temperature [36]. The contact pressure $p(T, \dot{\varepsilon})$ should be normalised by the yield stress $\sigma_y(T, \dot{\varepsilon})$for the same values of $(T, \dot{\varepsilon})$. Hence the yield stress was fitted with a second degree polynomial law to estimate the values at strain rates comparable to those in scratch tests (10^{-2}–10^{2} s^{-1})

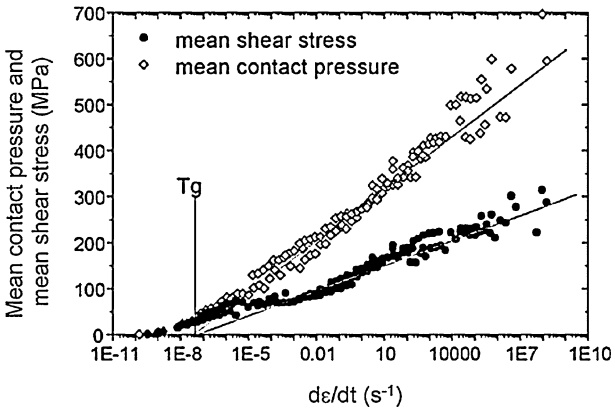

Fig. 16 Master curves for the apparent shear stress and contact pressure at a reference temperature of 20 °C. Scratch tests on PMMA were performed with a conical tip at temperatures in the range of – 50–115 °C

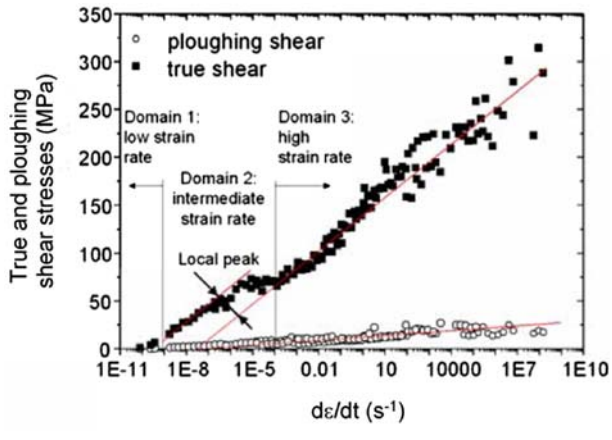

Fig. 17 Master curves for the ploughing and true shear stresses plotted at a reference temperature of 20 °C. Scratch tests on PMMA were performed with a conical tip at temperatures in the range – 50–115 °C

$$\sigma_y(\dot{\varepsilon}, T) = a(T) + b(T)\log\dot{\varepsilon} + c(T)(\log\dot{\varepsilon})^2 \quad (21)$$

Figure 18 shows this ratio versus the contact strain. Several tip geometries were used to scan a wide range of contact strains. Particular values of the normalised pressure indicate the boundaries of different behavioural domains corresponding to elastic, elastic–plastic or plastic contact [36]. As the coefficient of the friction between the tip and the surface reaches 0.3, plasticity appears under the contact surface and the normalised pressure is close to about 1 [37]. The strain, which is proportional to the ratio a/R, increases as the normal load increases. A plastic volume appears under the contact area and the normalised pressure also increases. The relationship between contact pressure and yield stress is already known for indentation tests, and the present work provides an equivalent relation for scratching. For plastic scratching, it was assumed that the normalised pressure is about 2 for polymers.

Figure 19 presents values of the true local friction as a function of the normalised pressure for sliding and scratching tests on PMMA. The true local friction shows an increase as the normalised pressure exceeds 1.1, i.e., as plasticity appears in the contact.

The increase of the true friction at high local pressure indicates that some unknown molecular mechanisms arises at the interface between the tip and the polymer. It may be some kind of local inter-phase made of modified polymer between the tip and the original bulk polymer: under high local pressure, one could expect some superficial orientation of the polymer, or even strong heating due to the dissipated friction energy in an extremely thin layer or polymer at the interface. The hypothetical temperature increase would increase the tack at the interface, increasing the friction coefficient.

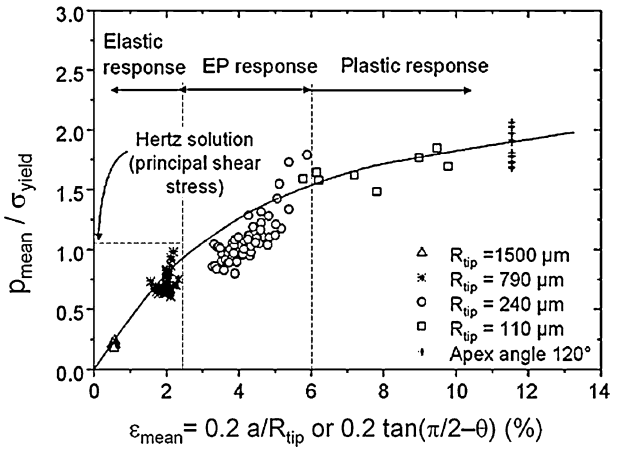

Fig. 18 Evolution of the normalised contact pressure as a function of the mean contact strain. Scratch tests and sliding tests on PMMA were performed with various tip at temperatures in the range 20–100 °C and at sliding speeds in the range 1 µm/s–15 mm/s

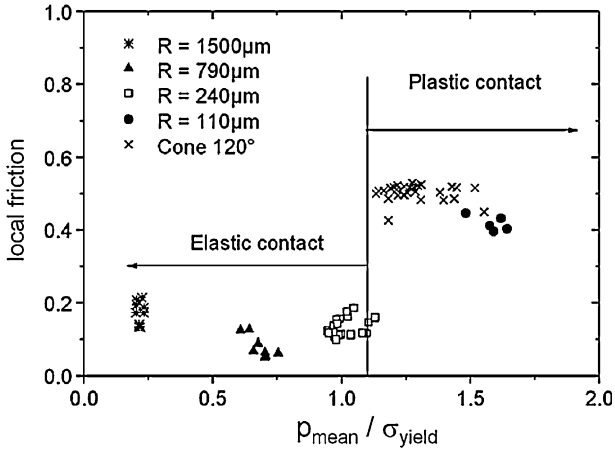

Fig. 19 Evolution of the true local friction as a function of the normalised pressure in sliding and scratching tests on PMMA (4 decades of velocity and room temperature)

Conclusions

Polymer friction shows a large dependence on temperature and sliding speed. The origin of this dependence is often attributed to surface thermodynamics while neglecting the influence of the contact mechanics. Flow line models previously presented have now been used to identify the components of the local and ploughing frictions.

The apparent friction and true local friction show peaks correlated with the loss factor, while the ploughing friction is linked to the contact dissymmetry, which has a viscoelastic or plastic origin. The physical origin of the ploughing friction peak resides in the variation of the contact shape, itself related to the evolution of the loss factor. Adhesion hysteresis appears to be responsible for the true local friction. Other parameters acting on the true local friction are the contact time and temperature.

A shear stress master curve may be plotted. The inconvenience of this representation is to mask the behavioural transitions or friction peaks, which appear at low contact pressure when the glass temperature is reached.

Appendix

Calculation of the ploughing friction for a hyperbolic rear contact edge

The ploughing friction for a zero true local friction is the ratio of the tangential S_t to the normal contact area S_n· S_t is delimited

(a) by the intersection of the conical shape $x^2 + y^2 - (z\tan\theta)^2 = 0$ and the rear plane $x = r\sin\omega$, where S_t is part of the section included in the hyperbola (H)

$$-\frac{y^2}{p^2}+\frac{z^2}{q^2}-1=0$$

with $p = r\sin\omega$ and $q = r\sin\omega/\tan\theta$, and
(b) by the plane $z = -r/\tan\theta$.

S_t is calculated from

$$S_t = 2p\int_{z_1}^{z_2}\sqrt{\frac{z^2}{q^2}-1}\,\mathrm{d}z$$

with the integration limits $z_1 = -r/\tan\theta$ and $z_2 = -r\sin\omega/\tan\theta$.

If $z = q/\sin\varphi$, then $S_t = -2pq\int\frac{\mathrm{d}\varphi}{\sin^3\varphi}+2pq\int\frac{\mathrm{d}\varphi}{\sin\varphi}$ and if $t = \tan\varphi/2$ where $\sin\varphi = \frac{2t}{1+t^2}$, then

$$S_t = \frac{2r^2\sin^2\omega}{\tan\theta}\left[\frac{1}{8}\left(\tan^2\varphi/2-\frac{1}{\tan^2\varphi/2}\right)-\frac{1}{2}\ln|\tan\varphi/2|\right]_{z_1}^{z_2}$$

where

$$\tan\varphi/2 = \frac{1-\sqrt{1-\frac{r^2\sin^2\omega}{\tan^2\theta z^2}}}{\frac{r\sin\omega}{\tan\theta z}}$$

The normal contact area is $S_n = (\pi + 2\omega + \sin 2\omega)r^2/2$ and the general form of Tabor's ploughing friction coefficient is

$$\mu_{\text{plough}} = 4\cot\theta\frac{\sin^2\omega}{(\pi+2\omega+\sin 2\omega)}f(\varphi)$$

where

$$f(\varphi) = \left[\frac{1}{8}\left(\tan^2\varphi/2-\frac{1}{\tan^2\varphi/2}\right)-\frac{1}{2}\ln|\tan\varphi/2|\right]_{-r/\tan\theta}^{-r\sin\omega/\tan\theta}$$

like $f(\varphi)$ depends on $\tan\theta$, $f(\varphi) = g(\theta)$. Hence there is no analytical expression for the general case of the exact solution of the ploughing friction coefficient in the form $\mu_{\text{plough}} = 2/\pi\cot\theta f(\omega)$.

References

1. Berthoud P, Baumberger T, G'sell C, Hiver JM (2001) Phys Rev B 59(22):14313
2. Baumberger T, Berthoud P, Caroli C (2001) Phys Rev B 60(6):3928
3. Greenwood JA, Williamson JB (1966) Proc Roy Soc A 295:300
4. Bowden FP, Tabor D (1951) In: Friction and lubrication of solids. Oxford University Press, London
5. Johnson KL, Kendall K, Roberts AD (1971) Proc R Soc Lond A 324:301
6. Dejarguin BV, Muller VM, Toporov YUP (1975) J Colloïd Interface Sci 53:314
7. Maugis D (1996) J Adhesion Sci Technol 10(2):161
8. Yoshizawa H, Chen Y-L, Israelachvili J (1993) J Phys Chem 97:4128
9. Chaudhury MK, Owen MJ (1993) Langmuir 9:29
10. Jardret V, PhD, Ecole Centrale de Lyon, France, 1994
11. Bucaille JL, PhD, Ecole des Mines de Paris, France, 2001
12. Gauthier C, Schirrer R (2000) J Mater Sci 35:2121
13. Briscoe BJ (1986) In: Friedrich K (ed) Composite materials series 1. Elsevier, p 25
14. Moore DF (1972) The friction and lubrication of elastomers. Pergamon Press, London
15. Casoli A, Brendle M, Schultz J, Auray P, Reiter G (2001) Langmuir 17:388
16. Yamada S, Israelachvili J (1998) J Phys Chem B 102:234
17. Bhushan B (1999) Wear 225:465
18. Basire C, Fretigny C (1997) C R Acad Sci 325 II b:211
19. Khurshudov A, Kato K (1997) Wear 205:10
20. Zhang SL, Li JCM (2003) Mater Sci Eng A 344:182
21. Bowden FP, Tabor D (1966) J Appl Phys 17:1521
22. Briscoe BJ, Tabor D (1975) Wear 34:29
23. Briscoe BJ, Thomas PS (1995) Tribol Trans 38:382
24. Briscoe BJ, Stolarski T, Davis S (1984) Tribol Int 17:129
25. Bucaille JL, Gauthier C, Felder E, Schirrer R (2006) Wear 260:803
26. Bulgin D, Hubbard GD, Walters MH (1962) Proc. 4th Rubber Technology Conf., London, 173
27. Bueche AM, Flom DG (1959) Wear 2:168
28. Ludema KC, Tabor D (1966) Wear 9:329
29. Steijn RP (1986) In: Failure of plastics, chap 19, Hanser Publishers
30. Gauthier C, Lafaye S, Schirrer R (2001) Tribol Int 34:469
31. Bucaille J-L, Felder E, Hochstetter G (2001) Wear 249:422
32. Lafaye S, Gauthier C, Schirrer R (2005) Tribol Int 38:113
33. Goddard J, Wilman H (1962) Wear 5:114
34. Aklonis J, MacKnight W (1983) Introduction to polymer viscoelasticity. John Wiley and Sons
35. Briscoe BJ, Pelillo E, Shinha S (1996) Polym Eng Sci 36:2996
36. Gauthier C, Schirrer R (2001) The viscoelastic viscoplastic behaviour of a scratch on a polymeric surface. Proc of the 2nd World Tribology Congress WTC2001, Vienna Austria September 2001, CDROM
37. Johnson KL (1984) In: Contact mechanics. Cambridge University Press